ACS Catalysis

Research Article

pubs.acs.org/acscatalysis

Fabrication of Ag_3PO_4-Graphene Composites with Highly Efficient and Stable Visible Light Photocatalytic Performance

Xiaofei Yang,*[,†] Haiying Cui,[‡] Yang Li,[†] Jieling Qin,[†] Rongxian Zhang,[§] and Hua Tang*[,†]

[†]School of Materials Science and Engineering, [‡]School of Food and Biological Engineering, and [§]School of Chemistry and Chemical Engineering, Jiangsu University, Zhenjiang 212013, P. R. China

Supporting Information

ABSTRACT: A facile and effective hydrothermal method for the fabrication of the Ag_3PO_4-graphene (Ag_3PO_4-GR) visible light photocatalyst has been developed to improve the photocatalytic performance and stability of Ag_3PO_4, and also to reduce the high cost of Ag_3PO_4 for practical uses. The size and morphology of Ag_3PO_4 particles could be tailored by the electrostatically driven assembly of Ag^+ on graphene oxide (GO) sheets and by the controlled growth of Ag_3PO_4 particles on the GO surface. The generation of Ag_3PO_4 and the transformation of GO to GR can be achieved simultaneously in the hydrothermal process. The improved photocatalytic activity of Ag_3PO_4-GR composites under visible light irradiation is attributed to high-surface-area GR sheets, enhanced absorption of organic dyes, and more efficient separation of photogenerated electron−hole pairs. The transfer of photogenerated electrons from the surface of Ag_3PO_4 to GR sheets also reduces the possibility of decomposing Ag^+ to metallic Ag, suggesting an improved stability of recyclable Ag_3PO_4-GR composite photocatalyst. Moreover, with the advances in the large-scale production of high-quality GO, the use of GO as the starting material can also reduce the cost for the synthesis of Ag_3PO_4-based photocatalysts without weakening their photocatalytic activities.

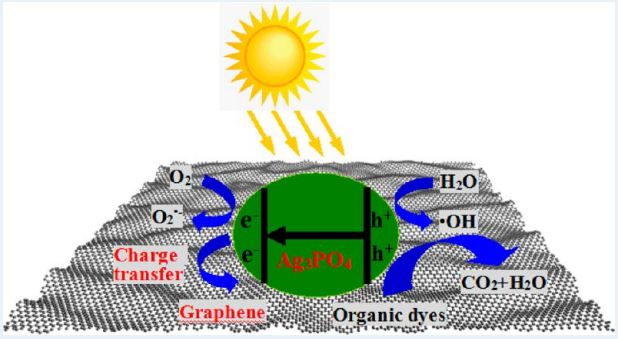

KEYWORDS: *graphene, Ag_3PO_4, composites, hydrothermal, visible light photocatalytic*

1. INTRODUCTION

Since the discovery of photocatalytic water splitting on titania by Fujishima and Honda in 1972,[1] significant effort has been devoted to the development of highly active photocatalysts. Of particular interest are photocatalysts that function with visible light, which have wide-ranging potential applications in areas such as water splitting for hydrogen production, removal and degradation of pollutants, and water purification and disinfection.[2,3] Most recently, it has been shown that silver orthophosphate (Ag_3PO_4) has extremely high photooxidative capabilities for O_2 generation from water splitting under visible-light irradiation.[4] Moreover, it has been reported that Ag_3PO_4 is an efficient visible-light photocatalyst for the degradation organic dyes.[5] Despite the fact that Ag_3PO_4 demonstrates highly efficient visible-light photocatalytic performance, one disadvantage is the high cost of the starting material, $AgNO_3$, which prohibits large-scale production. Ag_3PO_4 samples normally possess irregular polyhedral microstructures and have poor dispersity/solubility. The photocatalytic activity of Ag_3PO_4 has also been shown to be closely related to its size, morphology, and specific highly reactive facet, and is also affected by decomposition rates to metallic Ag in the photocatalytic process.

Over the past few years, more attention has been paid to morphology-controlled synthesis of Ag_3PO_4,[6−9] and to the preparation of Ag_3PO_4-based composite photocatalysts including TiO_2/Ag_3PO_4,[10,11] Fe_3O_4/Ag_3PO_4,[12] carbon quantum dots (CQDs)/Ag_3PO_4,[13] Ag/Ag_3PO_4,[14−16] AgX/Ag_3PO_4,[17,18] SnO_2/Ag_3PO_4,[19] and so forth. However, low-cost fabrication of well-defined Ag_3PO_4-based photocatalysts with superior photocatalytic properties via a simple process remains a great challenge.

Graphene (GR) has proven to be a promising candidate for the fabrication of visible-light-responsive photocatalytic composites.[20−30] It has been suggested that graphene may tailor the size and morphology of photocatalysts. Additionally, its conductive properties can also slow the recombination of photogenerated electron−hole pairs, consequently resulting in an enhancement in photocatalytic activity. Moreover, the cost for the synthesis of Ag_3PO_4-based photocatalysts can be greatly reduced with the recent improvements in the large-scale synthesis of graphene oxide (GO). Thus the fabrication of Ag_3PO_4 using GO as the precursor provides an exciting opportunity for the large-scale preparation of highly active Ag_3PO_4-GR composite photocatalysts. Most recently, two research groups and my group independently reported the

Received: December 13, 2012
Revised: January 18, 2013
Published: January 22, 2013

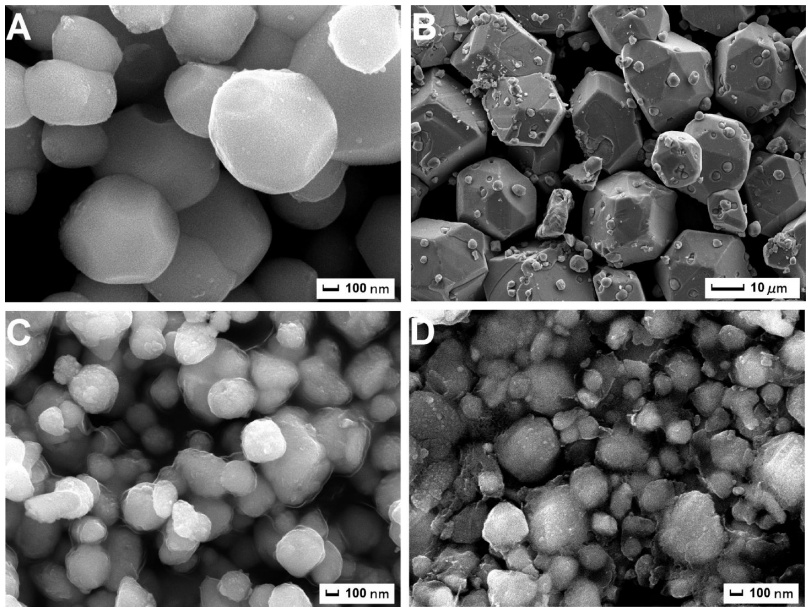

Figure 1. FESEM images of (A) Ag_3PO_4, (B) Ag_3PO_4-HT, (C) Ag_3PO_4-GO composites, and (D) Ag_3PO_4-GR composites.

synthesis of GO-Ag_3PO_4 composites with enhanced visible-light photocatalytic performance.[31−33] To the best of our knowledge, no previous studies regarding the hydrothermal synthesis and photocatalytic performance of Ag_3PO_4-GR composite photocatalysts have been reported. In the present work, well-defined Ag_3PO_4-GR hybrids with promising visible-light photocatalytic activity are synthesized by electrostatically driven self-assembly between positively charged Ag^+ and negatively charged GO sheets, followed by the addition of the precipitant disodium hydrogen phosphate (Na_2HPO_4) and hydrothermal treatment. The visible-light-driven photocatalytic activity of Ag_3PO_4-GR hybrids is investigated together with their structural and physicochemical properties.

2. EXPERIMENTAL SECTION

2.1. Materials and Sample Preparation. *Synthesis of GO Aqueous Suspension.* Graphite oxide was synthesized from graphite purchased from Sinopharm Chemical Reagent Co. Ltd. (Shanghai, China), using the improved Hummers method with additional $KMnO_4$.[34] In a typical synthesis, Graphite (3 g) was first ground with NaCl (50 g) for 30 min, followed by the removal of NaCl by repeatedly rinsing with deionized water; the remaining graphite was heated at 80 °C for 1 h. Concentrated H_2SO_4 (69 mL) was then added to a mixture of the dried graphite and $NaNO_3$ (1.5 g) in a 250 mL round-bottom flask; the mixture was stirred and kept at 0 °C for 2 h. $KMnO_4$ (9 g) was added dropwise to keep the reaction temperature below 20 °C. The reaction was warmed to 35 °C and stirred for 10 h. Additional $KMnO_4$ (9 g) was added, and the solution was allowed to stir for 12 h at 35 °C. Afterward, the reaction mixture was cooled to room temperature and poured into ice with H_2O_2 (30%, 3 mL) to end the reaction. The suspension was then centrifuged (10000 rpm) and the supernatant was decanted away; the remaining material was then repeatedly washed in succession with deionized water, HCl solution (3 M), and absolute ethanol. The obtained solid was collected and vacuum-dried overnight, obtaining 5.4 g of brown powder. The as-made graphite oxide (50 mg) was dispersed into distilled water (50 mL), and sonicated for 5 h to give a GO aqueous suspension (1.0 mg mL^{-1}).

Synthesis of Ag_3PO_4-GO Composites and Ag_3PO_4-GR Composites. In a typical synthesis, $AgNO_3$ aqueous solution (10 mL, 0.6 M) was added with stirring to the above GO aqueous suspension (50 mL,1.0 mg mL^{-1}); after the addition, the mixed suspension was kept stirring for further 12 h to ensure the electrostatically driven assembly of positively charged Ag^+ on the surface of negatively charged GO sheets. Then Na_2HPO_4 aqueous solution (10 mL, 0.2 M) was added dropwise to the mixture, and the reaction mixture was kept stirring for 30 min. Ag_3PO_4-GO composites were obtained by the direct collection of the precipitates by filtration and drying of the product in vacuum. For Ag_3PO_4-GR composites, the above mixed suspension was transferred into a 100 mL Teflon-lined stainless steel autoclave and kept in an oven at 180 °C for 24 h. The autoclave was left to cool naturally to room temperature, the obtained precipitate was collected by centrifugation, washed several times with absolute ethanol, and dried at 60 °C in vacuum overnight.

Synthesis of Ag_3PO_4 and Ag_3PO_4-HT. In a typical synthesis, Na_2HPO_4 aqueous solution (10 mL, 0.2 M) was added dropwise to the aqueous solution of $AgNO_3$ (10 mL, 0.6 M), and the obtained golden yellow precipitates were collected by filtration, washed with distilled water repeatedly, and dried in vacuum. The Ag_3PO_4-HT sample was prepared by the hydrothermal treatment of the mixture of Na_2HPO_4 aqueous solution (10 mL, 0.2 M) and $AgNO_3$ (10 mL, 0.6 M) aqueous solution at 180 °C for 24 h, followed by the collection of the precipitates by filtration and drying of the product in vacuum.

2.2. Characterization. The morphologies of the as-synthesized samples were examined by field-emission scanning electron microscopy (FESEM, JEOL, JSM-7001F). The phases of the obtained products were collected on a Bruker D8 Advance X-ray diffractometer (Cu K α radiation, λ = 0.15406 Å in a 2θ range from 10° to 80° at room temperature. Raman experiments were performed using a DXR spectrometer using the 532 nm laser line, and measurements were made in backscattering geometry. UV−visible diffuse reflectance spectra

dx.doi.org/10.1021/cs3008126 | ACS Catal. 2013, 3, 363−369

Scheme 1. Schematic Illustration of the Synthesis Procedures of Ag_3PO_4, Ag_3PO_4-HT, Ag_3PO_4-GO, and Ag_3PO_4-GR Composites

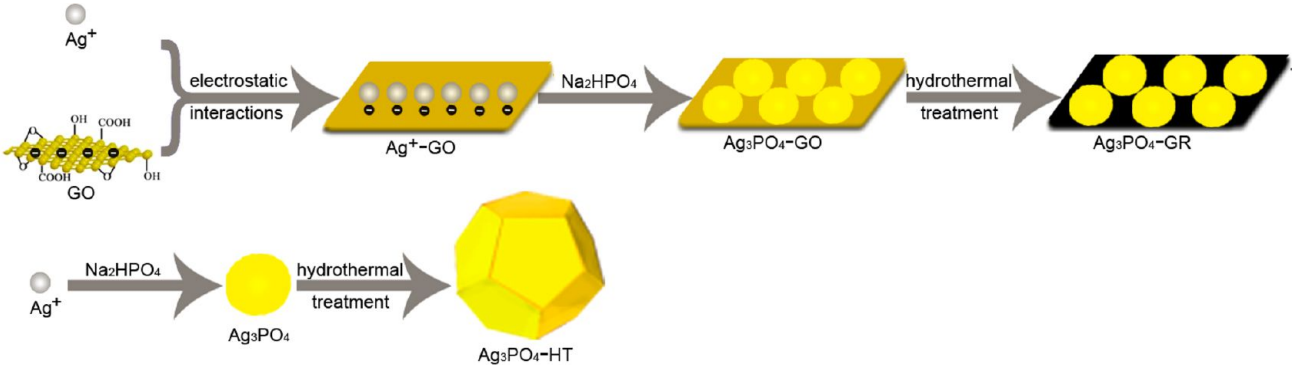

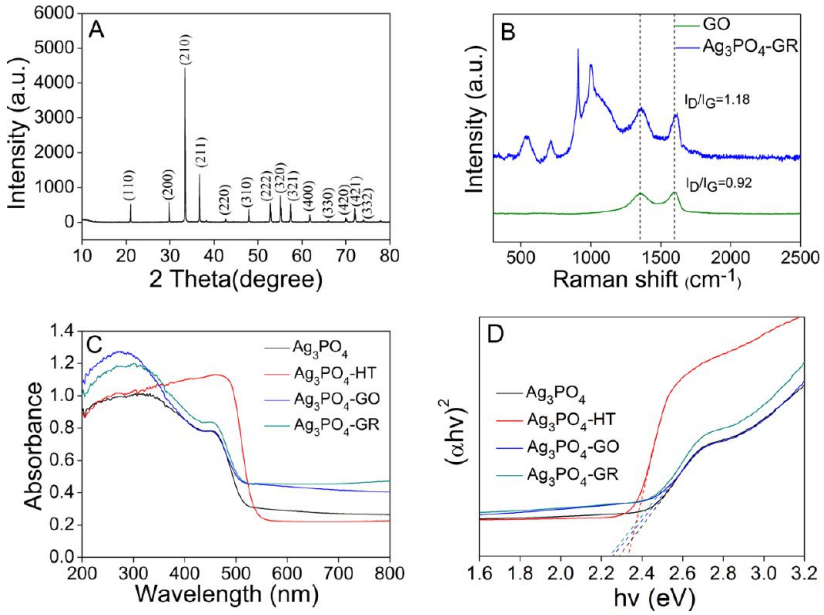

Figure 2. (A) XRD pattern of Ag_3PO_4-GR composites; (B) Raman spectra of Ag_3PO_4-GR composites and GO; (C) UV−vis diffuse reflectance spectra, and (D) the plot of $(\alpha hv)^2$ versus energy (hv).

were recorded within the 200−800 nm wavelength range using a Shimadzu UV2450 spectrometer. Electron spin resonance (ESR) spectra were recorded at 77 K with an ESR spectrometer (Bruker, ESP-300E) for the sample (20 mg) in liquid nitrogen under irradiation with a 500 W mercury lamp.

2.3. Photocatalytic Experiment. The optical system for the photocatalytic reaction was composed of a 350 W Xe lamp and a cutoff filter (λ>420 nm). Dye solutions (100 mL, 10^{-5} mol/L) containing 50 mg of samples were put in a sealed glass beaker and first ultrasonicated for 10 min, and then stirred in the dark for 30 min to ensure absorption−desorption equilibrium. After visible light illumination, 4 mL of samples were taken out at regular time intervals (0.5 min) and separated through centrifugation (10000 rpm, 10 min). The supernatants were analyzed by recording variations of the absorption band maximum in the UV−vis spectra by using a Lambda 25 UV/vis spectrophotometer.

3. RESULTS AND DISCUSSION

3.1. Characterization of As-Prepared Samples. The morphology and structure of as-prepared samples are first characterized by field-emission scanning electron microscopy (SEM). It can be seen in Figure 1A that as-prepared Ag_3PO_4 possesses an irregular sphere-like polyhedral morphology with an average diameter of 450 nm. As shown in Figure 1B, Ag_3PO_4 polyhedra with an average diameter of more than 15 μm were observed when the mixed aqueous solution comprising silver nitrate ($AgNO_3$) and disodium hygrogen phosphate (Na_2HPO_4) was sealed in an autoclave and hydrothermally treated at 180 °C for 24 h, indicating that hydrothermal treatment of the sample results in a remarkable increase in the size of Ag_3PO_4 polyhedra. Interestingly, when 50 mg of GO (1 mg/mL) aqueous dispersion was introduced into this synthetic system (without hydrothermal treatment), Ag_3PO_4-GO composites were obtained; in this process, first, electrostatic properties drive the self-assembly of positively charged Ag^+ and negatively charged GO sheets, followed by the generation of Ag_3PO_4 seed particles and controlled growth of Ag_3PO_4 particles on the surface of GO sheets. An FESEM image of Ag_3PO_4-GO composites (Figure 1C) clearly reveals that it consists of sphere-like Ag_3PO_4 polyhedra with an average diameter of 250 nm, and most particles are observed to be coated by flexible GO sheets. FESEM observations imply that the presence of GO has an obvious effect on the morphology of

dx.doi.org/10.1021/cs3008126 | ACS Catal. 2013, 3, 363−369

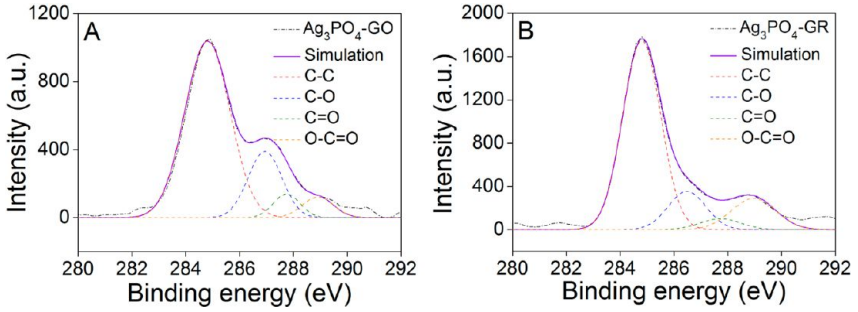

Figure 3. XPS spectra of C 1s for (A) Ag_3PO_4-GO and (B) Ag_3PO_4-GR composites.

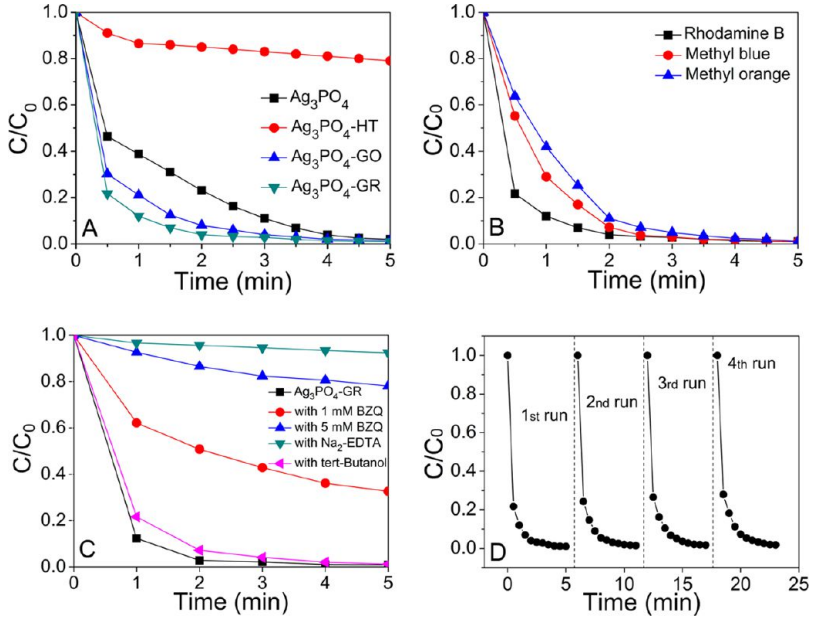

Figure 4. Photocatalytic activity of (A) samples for RhB degradation under visible light irradiation; (B) Ag_3PO_4-GR composites for RhB, MB, and MO; (C) reactive species trapping experiments and (D) repeated photocatalytic experiments of Ag_3PO_4-GR composites.

Ag_3PO_4 particles. Moreover, hydrothermal treatment of Ag_3PO_4-GO composites at 180 °C for 24 h leads to transformation of Ag_3PO_4-GO composites to Ag_3PO_4-GR composites and causes a slight decrease in the size of Ag_3PO_4 particles in the Ag_3PO_4-GR composites (Figure 1D). A procedure for the synthesis of different samples is illustrated in Scheme 1.

The X-ray diffraction (XRD) pattern (Figure 2A) clearly shows that all of the diffraction peaks of the Ag_3PO_4-GR composite could be readily indexed to the body-centered cubic structure of Ag_3PO_4 (JCPDS No. 06-0505). No characteristic diffraction peaks for graphene are observed in the pattern because of the low amount and the relatively low diffraction intensity of graphene. The presence of graphene and Ag_3PO_4 are further supported by Raman spectroscopy. It can be seen from Figure 2B that several peaks below 1300 cm^{-1} correspond to the vibrations of Ag_3PO_4. The two peaks at 1350 cm^{-1} (D peak) and 1590 cm^{-1} (G peak) are attributed to GR. In comparison with GO (I_D/I_G = 0.92), an increased D/G intensity ratio (I_D/I_G = 1.18) was observed, suggesting the reduction of GO to GR. XRD pattern, Raman spectrum, and TEM image of as-prepared GO were also recorded as reference (Supporting Information, Figure S1). Furthermore, a comparison of the UV−vis diffuse reflectance spectra of four samples are displayed in Figure 2C. There is an obvious enhanced absorbance in the visible-light region (>500 nm) when Ag_3PO_4 was incorporated with GO or GR, compared with the spectrum of Ag_3PO_4. Hydrothermally treated Ag_3PO_4 exhibited a decreased visible-light absorbance in comparison with three samples. A plot of the transformed Kubelka−Munk function of light energy $(\alpha h\nu)^2$ versus energy ($h\nu$) is also shown in Figure 2D. From this, the band gaps of the samples were estimated to be 2.23 eV, 2.35 eV, 2.28 eV, and 2.33 eV corresponding to Ag_3PO_4-GR composite, Ag_3PO_4-GO composite, Ag_3PO_4, and Ag_3PO_4-HT, respectively. Band gap narrowing was clearly observed for Ag_3PO_4-GR composites and Ag_3PO_4-GO composites. By contrast, a broadened band gap of Ag_3PO_4-HT was observed.

To investigate the transformation of GO to GR in the hydrothermal reduction process, XPS spectra of C1s were collected for Ag_3PO_4-GO and Ag_3PO_4-GR samples (Figure 3). The XPS spectrum of C1s for Ag_3PO_4-GO composites (Figure 3A, solid line) can be deconvoluted into four peaks (dashed lines), which are attributed to the following functional groups: sp^2 bonded carbon (C−C, 284.8 eV), epoxy/hydroxyls (C−O, 286.9 eV), carbonyls (C═O, 287.8 eV), and carboxyl (O−C═O, 288.9 eV). Four peaks for C−C, C−O, C═O, and O−C═O (dashed lines) still exist in the XPS spectrum of C1s for Ag_3PO_4-GR composites (Figure 3B, solid line); however, the percentage of oxygen-containing functional groups decreases.

dx.doi.org/10.1021/cs3008126 | ACS Catal. 2013, 3, 363−369

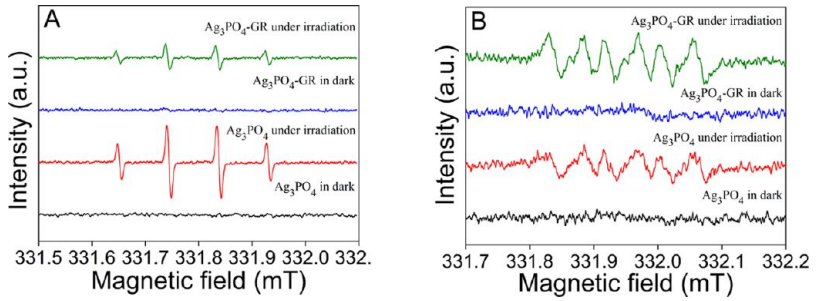

Figure 5. ESR spectra of radical adducts trapped by DMPO in Ag_3PO_4-GR aqueous dispersions (A) and methanol dispersions (B).

The degree of reduction of GO has also been quantified by calculating the relative content of carbon in the samples, indicating that Ag_3PO_4-GO composites have 54% graphitic carbon and 46% oxidized carbon. With Ag_3PO_4-GR composites, 72% graphitic carbon and 28% oxidized carbon were found. The results further confirmed the loss of oxygen-containing functional groups and the transformation of Ag_3PO_4-GO composites to Ag_3PO_4-GR composites by hydrothermal reduction; full and Ag 3d XPS spectra from Ag_3PO_4-GR composites are provided (Supporting Information, Figure S2).

3.2. Photocatalytic Degradation Results and Analysis. Furthermore, the photocatalytic performance of the samples was measured using the degradation of organic dyes under visible-light irradiation as a model reaction, and the results are shown in Figure 4.

To the best of our knowledge, this is the first example in which Ag_3PO_4-GR composites have been used as visible-light photocatalysts. The photocatalytic performances of as-prepared Ag_3PO_4, Ag_3PO_4-HT, and Ag_3PO_4-GO composites were also investigated for comparison. Figure 4A shows that all Ag_3PO_4-based materials exhibited excellent photocatalytic activities in the degradation of RhB except the hydrothermally treated sample, Ag_3PO_4-HT. Among them, Ag_3PO_4-GR composites presented the highest visible-light photocatalytic performance with the efficiency of nearly 100% in 2 min. Three minutes is needed for Ag_3PO_4-GO composites, and 4 min is needed for Ag_3PO_4 polyhedra. Ag_3PO_4-GR was further used for the degradation of three different organic dyes, rhodamine B (RhB), methyl blue (MB), and methyl orange (MO), under the same conditions. The results indicate that a higher photocatalytic degradation rate was achieved for RhB compared to MB and MO (Figure 4B).

Furthermore, reactive species trapping experiments were performed to investigate the reactive oxygen species in the photocatalytic process. In this study, three different chemicals, *p*-benzoquinone (BZQ, a $O_2^{-\bullet}$ radical scavenger), disodium ethylenediaminetetraacetate (Na_2-EDTA, a hole scavenger) and *tert*-butanol (a ·OH radical scavenger), were employed. The experimental results (Figure 4C) show that the addition of 1 mM BZQ reduced the photocatalytic activity for the degradation of RhB from almost 100% to 49% in 2 min. The photocatalytic degradation activity was further decreased to 13% after 2 min when a higher concentration of BZQ (5 mM) was employed. The introduction of 1 mM Na_2-EDTA into the same system caused fast deactivation of the Ag_3PO_4-GR photocatalyst, whereas the presence of *tert*-butanol had no deleterious effect on the photocatalytic activity. One possibility is that EDTA anion can be absorbed on the surface of the photocatalyst and acts as a hole trap or electron donor, resulting in the deactivation of the Ag_3PO_4-GR photocatalyst. The addition of BZQ to the Ag_3PO_4-GR photocatalytic system results in the capture of irradiated $O_2^{-\bullet}$ by BZQ and the decrease in the amount of active $O_2^{-\bullet}$ radicals for photocatalytic reactions. However, the fact that *tert*-butanol has no obvious effect on the photocatalytic activity, implies that $O_2^{-\bullet}$ radicals and holes contribute to photocatalytic perfromance and ·OH radicals do not. The robustness of the Ag_3PO_4-GR photocatalyst was confirmed by repeated photocatalytic experiments using a recycled catalyst sample under the same reaction conditions. As shown in Figure 4D, the experiments revealed that the photocatalytic efficiency remained consistently high.

Figure 5 shows electron spin resonance (ESR) spin-trap signals (with DMPO) of Ag_3PO_4-GR composites in two different dispersions. Figure 5A shows that four characteristic peaks of DMPO-·OH were observed in aqueous dispersions of Ag_3PO_4 and Ag_3PO_4-GR composites under visible light irradiation; no such signals were detected in the dark. However, signal intensities of ·OH radicals in Ag_3PO_4-GR composites are much weaker than those in Ag_3PO_4. Furthermore, the DMPO-$O_2^{-\bullet}$ species were also detected in methanol dispersions of two samples where 6 characteristic peaks of the DMPO-$O_2^{-\bullet}$ adducts were observed under visible light irradiation (Figure 5B); again no such signals were detected in dark in either case. Signal intensities of $O_2^{-\bullet}$ radicals in Ag_3PO_4-GR composites are stronger than those in Ag_3PO_4. ESR results indicated that certain visible light irradiation is crucial to the generation of ·OH radical and $O_2^{-\bullet}$ radical species and directly confirmed that both $O_2^{-\bullet}$ and ·OH are produced on the surface of visible light-irradiated Ag_3PO_4-GR composites, with $O_2^{-\bullet}$ radicals as the predominant species.

3.3. Possible Mechanism. Furthermore, XRD spectra of Ag_3PO_4 and Ag_3PO_4-GR samples after repeated visible light photocatalytic experiments were also recorded to understand the photocatalytic mechanism of Ag_3PO_4-GR composites. It is clearly shown in Figure 6 (top) that Ag_3PO_4 is partially decomposed to Ag. In contrast, no obvious signal from metallic Ag was observed with the Ag_3PO_4-GR sample after repeated photocatalytic measurements, confirming a higher photocatalytic stability of Ag_3PO_4-GR composites compared to pure Ag_3PO_4.

On the basis of the results described above, we propose the following mechanism (Figure 6, bottom). Under visible light irradiation, the electron−hole pairs of the Ag_3PO_4 semiconductor (conduction band: 0.45 eV, valence band: 2.45 eV) are separated, and the electrons at the valence band (VB) are excited to the conduction band (CB), inducing the formation of holes in the VB. $O_2^{-\bullet}$ radicals are produced by the reduction of O_2 molecules adsorbed on the catalyst surface by the

dx.doi.org/10.1021/cs3008126 | ACS Catal. 2013, 3, 363−369

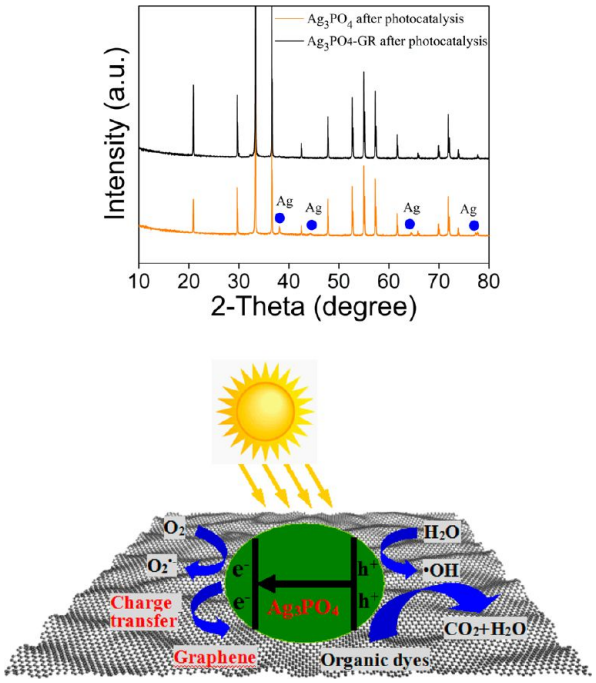

Figure 6. XRD spectra of Ag_3PO_4 and Ag_3PO_4-GR samples after visible light photocatalysis (top) and proposed photocatalytic mechanism of Ag_3PO_4-GR composites (bottom).

photogenerated electrons; because of the presence of conductive graphene sheets, charge transfer may also happen between separated photogenerated electrons and graphene in Ag_3PO_4-GR composites. In addition, the reaction of H_2O and active holes generate •OH, and both $O_2^{-\bullet}$ and •OH radicals can degrade organic dyes (RhB, MB or MO) effectively under visible light irradiation; furthermore, reactive holes at the VB are able to oxidize organic dye directly because of its strong oxidation. GR exhibited a significant influence on the photocatalytic activity for two reasons. First, high-surface-area GR sheets offer more active adsorption sites and photocatalytic reaction sites, which favor improved photocatalytic activity. Second, because of the presence of conductive GR sheets, it can serve as an effective acceptor of the photoexcited electrons; hence, the photogenerated CB electrons of Ag_3PO_4 can be transferred to GR sheets in the Ag_3PO_4/GR composite. The transportation and mobility of electrons on GR sheets are very rapid in the specific π-conjugated structure; thus the efficient electron transfer from Ag_3PO_4 to GR sheets keeps electrons away from the Ag_3PO_4. More photogenerated electrons and holes are produced by continuously working in this way, effectively suppressing the charge recombination and improving the photocatalytic activity, which reduces the decomposition rates of Ag^+ to metallic Ag in the photocatalytic process and suggests a better stability and recyclability of Ag_3PO_4/GR composites in the photocatalytic process.

4. CONCLUSIONS

In summary, we have developed a novel electrostatically driven hydrothermal approach to synthesize Ag_3PO_4-GR composites with controlled morphology. The choice of hydrophilic GO as the precursor proved to be crucial for the generation of well-defined Ag_3PO_4-GR composites. Our Ag_3PO_4-GR composites have superior visible-light-driven photocatalytic performance and are robust, offering a new method for the low-cost, large-scale production of visible-light active photocatalysts.

■ ASSOCIATED CONTENT

Supporting Information

XRD pattern, Raman spectrum, and TEM image of GO; XPS spectra of Ag_3PO_4-GO composites and Ag 3d for the sample; Visible light photocatalytic activity of Ag_3PO_4-GR composites for RhB with different concentrations; Pictures of the suspensions of as-prepared samples 10 min (top) and 2 h (bottom) after ultrasonication for 1 h. This material is available free of charge via the Internet at http://pubs.acs.org.

■ AUTHOR INFORMATION

Corresponding Author

*E-mail: xyang@ujs.edu.cn (X.Y.), tanghua@ujs.edu.cn (H.T.).

Notes

The authors declare no competing financial interest.

■ ACKNOWLEDGMENTS

The authors wish to express their sincere thanks to Keary Mark Engle, The Scripps Research Institute, U.S.A. and University of Oxford, U.K., and Dr. Zhanghua Gao of the University of Oxford for kindly reading and polishing this manuscript. This work was financially supported by the National Natural Science Foundation of China (51102116), Natural Science Foundation of Jiangsu (BK2011480, BK2011534), a Project Funded by Priority Academic Program Development of Jiangsu Higher Education Institutions, China Postdoctoral Science Foundation (2012M511223), Natural Science Foundation of the Jiangsu Higher Education Institutions of China (10KJB430001,12KJB550002) and Scientific Research Foundation for Advanced Talents, Jiangsu University (10JDG057, 11JDG050).

■ REFERENCES

(1) Fujishima, A.; Honda, K. *Nature* **1972**, *238*, 37−38.
(2) Kubacka, A.; Fernandez-Garcia, M.; Colon, G. *Chem. Rev.* **2012**, *112*, 1555−1614.
(3) Tong, H.; Ouyang, S. X.; Bi, Y. P.; Umezawa, N.; Oshikiri, M.; Ye, J. H. *Adv. Mater.* **2012**, *24*, 229−251.
(4) Yi, Z. G.; Ye, J. H.; Kikugawa, N.; Kako, T.; Ouyang, S. X.; Stuart-Williams, H.; Yang, H.; Cao, J. Y.; Luo, W. J.; Li, Z. S.; Liu, Y.; Withers, R. L. *Nat. Mater.* **2010**, *9*, 559−564.
(5) Bi, Y. P.; Ouyang, S. X.; Umezawa, N.; Cao, J.; Ye, J. H. *J. Am. Chem. Soc.* **2011**, *133*, 6490−6492.
(6) Liang, Q. H.; Ma, W. J.; Shi, Y.; Li, Z.; Yang, X. M. *CrystEngComm.* **2012**, *14*, 2966−2973.
(7) Khan, A.; Qamar, M.; Muneer, M. *Chem. Phys. Lett.* **2012**, *519−20*, 54−58.
(8) Bi, Y. P.; Hu, H. Y.; Ouyang, S. X.; Lu, G. X.; Cao, J. Y.; Ye, J. H. *Chem. Commun.* **2012**, *48*, 3748−3750.
(9) Wang, W. G.; Cheng, B.; Yu, J. G.; Liu, G.; Fan, W. H. *Chem.—Asian J.* **2012**, *7*, 1902−1908.
(10) Yao, W. F.; Zhang, B.; Huang, C. P.; Ma, C.; Song, X. L.; Xu, Q. J. *J. Mater. Chem.* **2012**, *22*, 4050−4055.
(11) Rawal, S. B.; Sung, S. D.; Lee, W. I. *Catal. Commun.* **2012**, *17*, 131−135.
(12) Li, G. P.; Mao, L. Q. *RSC Adv.* **2012**, *2*, 5108−5111.
(13) Zhang, H. C.; Huang, H.; Ming, H.; Li, H. T.; Zhang, L. L.; Liu, Y.; Kang, Z. H. *J. Mater. Chem.* **2012**, *22*, 10501−10506.
(14) Liu, Y. P.; Fang, L.; Lu, H. D.; Liu, L. J.; Wang, H.; Hu, C. Z. *Catal. Commun.* **2012**, *17*, 200−204.
(15) Liu, Y. P.; Fang, L.; Lu, H. D.; Li, Y. W.; Hu, C. Z.; Yu, H. G. *Appl. Catal., B* **2012**, *115*, 245−252.

(16) Bi, Y. P.; Hu, H. Y.; Ouyang, S. X.; Jiao, Z. B.; Lu, G. X.; Ye, J. H. *J. Mater. Chem.* **2012**, *22*, 14847−14850.
(17) Cao, J.; Luo, B. D.; Lin, H. L.; Xu, B. Y.; Chen, S. F. *J. Hazard. Mater.* **2012**, *217*−*218*, 107−115.
(18) Bi, Y. P.; Ouyang, S. X.; Cao, J. Y.; Ye, J. H. *Phys. Chem. Chem. Phys.* **2011**, *13*, 10071−10075.
(19) Zhang, L. L.; Zhang, H. C.; Huang, H.; Liu, Y.; Kang, Z. H. *New J. Chem.* **2012**, *36*, 1541−1544.
(20) An, X. Q.; Yu, J. C. *RSC Adv.* **2011**, *1*, 1426−1434.
(21) Xiang, Q. J.; Yu, J. G.; Jaroniec, M. *Chem. Soc. Rev.* **2012**, *41*, 782−796.
(22) Xiang, Q. J.; Yu, J. G.; Jaroniec, M. *J. Am. Chem. Soc.* **2012**, *134*, 6575−6578.
(23) Li, Q.; Guo, B. D.; Yu, J. G.; Ran, J. R.; Zhang, B. H.; Yang, H. J.; Gong, J. R. *J. Am. Chem. Soc.* **2011**, *133*, 10878−10884.
(24) Xiang, Q. J.; Yu, J. G.; Jaroniec, M. *Nanoscale* **2011**, *3*, 3670−3678.
(25) Wang, W. G.; Yu, J. G.; Xiang, Q. J.; Cheng, B. *Appl. Catal., B* **2012**, *119*−*120*, 109−116.
(26) Stankovich, S.; Dikin, D. A.; Dommett, G. H. B.; Kohlhaas, K. M.; Zimney, E. J.; Stach, E. A.; Piner, R. D.; Nguyen, S. T.; Ruoff, R. S. *Nature* **2006**, *442*, 282−286.
(27) Huang, X.; Qi, X. Y.; Boey, F.; Zhang, H. *Chem. Soc. Rev.* **2012**, *41*, 666−686.
(28) Zhang, J.; Yu, J. G.; Jaroniec, M.; Gong, J. R. *Nano Lett.* **2012**, *12*, 4584−4589.
(29) Xiang, Q. J.; Yu, J. G.; Jaroniec, M. *J. Phys. Chem. C* **2011**, *115*, 755−7363.
(30) Liu, S. W.; Liu, C.; Wang, W. G.; Cheng, B.; Yu, J. G. *Nanoscale* **2012**, *4*, 3193−3200.
(31) Liu, L.; Liu, J. C.; Sun, D. D. *Catal. Sci. Technol.* **2012**, *2*, 2525−2532.
(32) Liang, Q. H.; Shi, Y.; Ma, W. J.; Li, Z.; Yang, X. M. *Phys. Chem. Chem. Phys.* **2012**, *14*, 15657−15665.
(33) Cui, H. Y.; Yang, X. F.; Gao, Q. X.; Liu, H.; Li, Y.; Tang, H.; Zhang, R. X.; Qin, J. L.; Yan, X. H. *Mater. Lett.* **2013**, *93*, 28−31.
(34) Marcano, D. C.; Kosynkin, D. V.; Berlin, J. M.; Sinitskii, A.; Sun, Z. Z.; Slesarev, A.; Alemany, L. B.; Lu, W.; Tour, J. M. *ACS Nano* **2010**, *4*, 4806−4814.

NOTE ADDED AFTER ASAP PUBLICATION

After this paper was published ASAP on February 5, 2013, corrections were made to the text in section 2.1. The corrected version was reposted February 8, 2013.

dx.doi.org/10.1021/cs3008126 | *ACS Catal.* 2013, 3, 363−369